Micrometer scale spacings between fibronectin nanodots regulate cell morphology and focal adhesions

Utku Horzum, Berrin Ozdil and Devrim Pesen-Okvur

Izmir Institute of Technology, Department of Molecular Biology and Genetics, 35430 Izmir, Turkey

E-mail: devrimpesen@iyte.edu.tr

Abstract

Cell adhesion to extracellular matrix is an important process for both health and disease states. Surface protein patterns that are topographically flat, and do not introduce other chemical, topographical or rigidity related functionality and, more importantly, that mimic the organization of the *in vivo* extracellular matrix are desired. Previous work showed that vinculin and cytoskeletal organization are modulated by size and shape of surface nanopatterns. However, quantitative analysis on cell morphology and focal adhesions as a function of micrometer scale spacings of FN nanopatterns was absent. Here, electron beam lithography was used to pattern fibronectin nanodots with micrometer scale spacings on a K-casein background on indium tin oxide coated glass which, unlike silicon, is transparent and thus suitable for many light microscopy techniques. Exposure times were significantly reduced using the line exposure mode with micrometer scale step sizes. Micrometer scale spacings of 2, 4 and 8 μm between fibronectin nanodots proved to modulate cell adhesion through modification of cell area, focal adhesion number, size and circularity. Overall, cell behavior was shown to shift at the apparent threshold of 4 μm spacing. The findings presented here offer exciting new opportunities for cell biology research.

S Online supplementary data available from stacks.iop.org/MRX/1/025402/mmedia

Keywords: electron beam lithography, focal adhesion, fibronectin, cell shape

Introduction

Cell adhesion is an important process for both health and disease states such as wound healing and metastasis. Cells adhesion to the extracellular matrix (ECM) is mediated by focal adhesions (FA) involving proteins and complexes with sizes on the order of 10 nm to 10 μm. FAs are comprised of over a hundred proteins [1–4] where the basic modular structure contains an extracellular matrix protein (e.g. fibronectin), a transmembrane protein (integrins) and intracellular proteins (e.g. vinculin). Cell adhesion to ECM is widely studied using uniformly coated surfaces. However, ECM *in vivo* and ECM produced by cells *in vitro* have a complex structure with adhesive patches and non-adhesive spacings [5–9]. The dimensions of the former are at the nanometer scale, while those of the latter are at the micrometer scale ranging up to tens of micrometers. Surfaces that mimic the *in vivo* organization of the ECM should therefore have micrometer scale spacings in this range. In order to understand *in vivo* cell adhesion better, surfaces that closely mimic the *in vivo* ECM organization are needed.

There have been important cell adhesion studies using both micro and nanopatterned surfaces [10–23]. The pioneering contributions of Mirkin and Spatz are particularly noteworthy [24, 25]. However, there are limitations: although micropatterns can be fabricated with high throughput, they lack nanometer scale resolution and present large areas with uniform adhesiveness. On the other hand, most nanometer scale patterning processes lack pattern flexibility. In addition, they usually deliver a combination of topographical, biochemical and/or rigidity signals [10, 11, 17, 26, 27] rather than providing a pure biochemical signal, for example. While different types of signal are all crucial for cell response in order to dissect the contribution of each type of signal, surfaces that provide only that type of signal are essential. There have been significant previous studies on patterning proteins on surfaces; however, one drawback has been the presence of both biochemical and topography or stiffness signals due to the lack of a better fabrication method at the time. Oxide layers that inevitably introduce topography variations have been used to provide regions for protein versus polymer adsorption [26, 27]. In this case, the cells receive the biochemical signal (protein versus polymer) coupled to a topographical signal (high versus low regions on the surface). Thus, it would not be possible to assign the reason of a change in the cell response exclusively to a change in the surface topography or a change in the surface biochemistry. Gold nanoparticles coupled to polymers of various lengths have provided excellent control over distances between proteins; however, the method does not allow for patterns with varying spacings to be fabricated; the presence of gold particles also introduce additional signals for cell biology studies [11]. Electron beam lithography (EBL) has a resolution of a few nanometers due to a tightly focused electron beam (diameter ~2 nm).

EBL is a direct writing method that does not require the use of a photomask and can be used to fabricate patterns from a few nanometers to centimeters, covering the range of length scales that are important and practical for cell biological applications. EBL has been utilized to fabricate patterns of proteins on surfaces, and some of these patterned surfaces were also tested and shown to be functional at the cellular level [18, 26–35]. In one approach the resulting patterns present a purely biochemical signal because there are no differences in rigidity and the patterns are basically flat because adhesive patches have a thickness of only 2 nm [31]. This approach also uniquely makes it possible to pattern two proteins simultaneously since proteins are directly used as EBL resists [18]. Initial work using this approach used the focused electron beam to inactivate a surface bound protein such as fibronectin [34]. However, image reversal

was implemented to avoid the proximity effect and to be able to create nanometer scale patterns [36, 37]. The background is a protein layer and the pattern of interest is just another protein bound directly to the electron beam exposed regions on the background protein [31]. Using proteins directly as EBL resists without the need for PMMA, gold coating or beads, for example, yields a biochemical pattern devoid of topography or stiffness related inputs. Previous work also showed differences in vinculin and cytoskeleton organization in response to differently shaped FN nanopatterns, namely dot versus ring patterns on a K-casein background [18]. However, EBL patterning of proteins was performed on silicon substrates which are not transparent, thus limiting many downstream light microscopy applications important for cell biology assays. A quantitative analysis on cell morphology and focal adhesions as a function of micrometer scale spacings of FN nanopatterns was also absent in previous work. Here, indium tin oxide coated glass (ITO-glass) was used as substrate for direct patterning of surface immobilized proteins. The conductive nature of ITO-glass rendered it suitable for EBL and its transparency was advantageous for phase-contrast microscopy, a fundamental observation technique. The *in vivo* ECM was mimicked with nanometer scale FN dots with micrometer scale spacings. Immunostaining with FN specific antibodies and formation of pattern-specific FAs by breast cancer cells showed activity at the biochemical and cellular levels, respectively. In addition, the micrometer scale spacings of 2, 4 and 8 μm between FN nanodots proved to modulate cell adhesion through modification of cell morphology and FA features.

Methods

Unless otherwise noted, materials were obtained from Sigma, Germany.

Protein coating of ITO glass

ITO coated glass slides (whole or cut into 25 mm × 25 mm pieces) with ∼230 nm ITO coating and ∼8 ohm sqr^{-1} resistance (TEKNOMA, Izmir, Turkey) were cleaned with sequential sonication in acetone, isopropyl alcohol and ultra-pure (UP) water (18.2 mega-ohm), followed by UV/Ozone treatment (BioForce Nanosciences, Inc., USA). ITO-glass was incubated in 3% APTES solution (3-aminopropyl triethoxy-silane, in acetone) for 30 min. The APTES treated ITO-glass was rinsed with acetone, UP water, dried and baked in a 110 °C oven for 1 h. APTES coated ITO-glass was incubated in 0.5% glutaraldehyde for 15 min and rinsed just before incubation with 2 mg ml^{-1} K-casein for 24 h. K-casein coated ITO-glass was rinsed with buffer, UP water, dried and stored inside a desiccator. After EBL, K-casein:ITO-glass was backfilled with 0.05 mg ml^{-1} FN for 1 h, rinsed with buffer, UP water, dried and stored.

Electron beam lithography

K-casein coated ITO-glass was patterned by EBL using a Raith E-line system with a high precision interferometric stage (Raith GmbH, Dortmund, Germany). The accelerating voltage was set to 5 kV. Apertures of 7.5 and 30 μm gave typical beam currents of ∼15 and ∼150 pA, at a working distance of ∼10 mm. Patterns were designed using the Raith software in GDSII format. A range of area (5–100 μC cm^{-2}) and line (2–3200 pAs cm^{-1}) exposure doses were tested. Using micrometer scale step sizes in the line exposure mode significantly reduced exposure times. During electron beam exposure, samples were under a system vacuum of

$\sim$2–5 $\times$ 10^{-6} mBar for up to 16 h. The Raith system was also used to collect SEM images of patterned and immunostained FN:K-casein:ITO-glass samples at 5 kV.

Cell culture

All cell culture materials were obtained from Biological Industries, Israel. MDA-MB-231 cells were grown in DMEM with 10% fetal bovine serum (FBS) at 37 °C and 5% CO_2. Cells were passaged every 2–3 days. For experiments, cells ready for passaging were starved in serum free medium for 2 h, trypsinized and cultured in DMEM with FBS on ITO-glass with 0.6×10^6 cells per 60 mm petri dish at 37 °C and 5% CO_2 for 18 h.
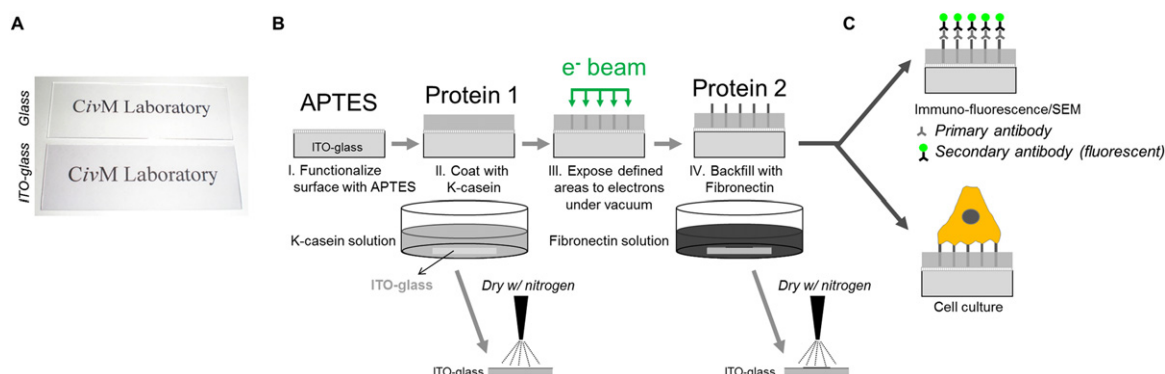
Immunofluorescence

FN:K-casein:ITO-glass without cells was directly processed for immunostaining. Surfaces with cells were fixed with 4% paraformaldehyde and permeabilized with 0.1% Triton X-100. The samples were blocked with 1% bovine serum albumin, stained for FN and vinculin using FN and vinculin specific primary antibodies, followed by Alexa488 or Alexa555 fluorophore conjugated secondary antibodies (Molecular Probes, Eugene, OR, USA). The samples were imaged using an Olympus epifluorescence microscope with a 100X oil immersion objective. Images were processed using ImageJ.

Image analysis

All image processing and analysis steps were performed using ImageJ. Cell contours were manually drawn. Vinculin images were processed through either 'Subtract background', 'CLAHE (Contrast Limited Adaptive Histogram Equalization)', 'Mathematical exponential(exp)' and 'Log3D' (figure 7 and online figure S2, available at stacks.iop.org/MRX/1/025402/mmedia) or 'Subtract background', 'Subtract' and 'Log3D' steps before thresholding (online figures S3 and S4, available at stacks.iop.org/MRX/1/025402/mmedia). Identified FAs were analyzed with 'Analyze Particles'. N = 5–9 cells or 7-416 FAs were analyzed per group. Different thresholds and background subtraction steps were tested but different paths only negligibly changed the absolute values for the parameters tested and the correlations between parameters were virtually the same (online figures S3 and S4, available at stacks.iop.org/MRX/1/025402/mmedia).
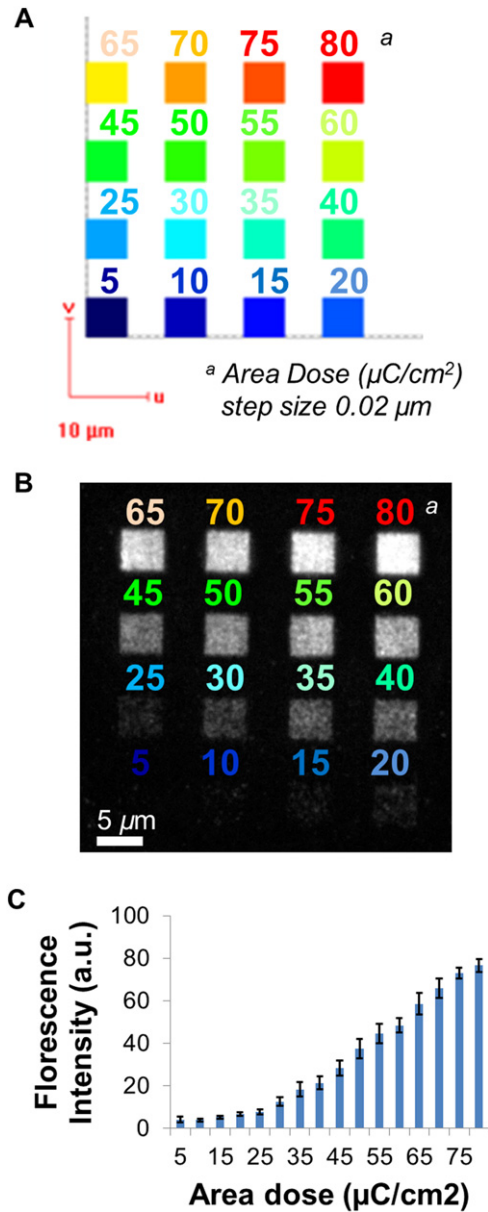
Results and discussion

Previous studies have shown that proteins can be used directly as EBL resists on silicon substrates [31]. However, silicon is not transparent and thus limits usage of many light microscopy based assays used in cell biology. To overcome these limitations, the suitability of ITO-glass as an EBL substrate with proteins as EBL resists was tested. EBL requires a conductive substrate. ITO-glass is conductive due to a thin layer of ITO coating which does not significantly change the transparency of the underlying glass (figure 1(A)). ITO-glass is also more affordable than silicon wafers. The fabrication process is outlined in figure 1(B). ITO-glass was first functionalized with APTES (3-aminopropyl triethoxy-silane) which induces protein binding. After coating the APTES treated ITO-glass with the protein of interest 1 (K-casein), the surface was exposed to a focused electron beam and finally backfilled with protein of interest 2 (FN). Patterned ITO-glass was then characterized at the biochemical and cellular levels (figure 1(C)).

Figure 1. Electron beam lithography based approach for fabricating proteins patterns on transparent ITO-glass. (A) Image of standard glass slide and ITO coated glass slide. Both are similarly transparent and the words underneath are clearly visible. (B) ITO-glass surfaces are functionalized with APTES before coating with K-casein. A focused electron beam is raster scanned on the K-casein:ITO-glass surface which is then incubated with FN. (C) FN localization is determined using immunofluorescence, which is performed with antibodies that specifically recognize FN (⊥) and secondary fluorescent antibodies (⊥) that specifically recognize the former (⊥). Bioactivity is assayed at the cellular level.

Suitability of ITO-glass for direct patterning of protein coated surfaces using EBL was first tested on K-casein:ITO-glass using the area exposure mode (figure 2). Area doses ranging from 5 to $80 \, \mu C \, cm^{-2}$ were tested. After EBL, the surface was backfilled with and immunostained for FN. Results showed that first, K-casein coated ITO-glass can be directly patterned with EBL where FN selectively binds to the exposed areas on K-casein. Second, FN nanodots patterned on K-casein:ITO-glass can be detected by FN immunospecific antibodies. Third, the mean intensity as well as the homogeneity of the immunofluorescence signal for FN on the electron beam exposed areas increased as the applied electron dose increased, consistent with previous results on silicon substrates [31]. Area doses as low as $5 \, \mu C \, cm^{-2}$ initiated FN binding but efficient coverage of the exposed area by FN was observed at area doses of $65 \, \mu C \, cm^{-2}$ and higher. Previous work showed that electron beam irradiation does not change surface topography but rather surface functionality, as determined by phase imaging with atomic force microscopy [31]. The exact chemical nature of the change induced by the focused electron beam on K-casein is not known; however, it is likely to show similarities to changes previously reported on self-assembled monolayers [33, 38].
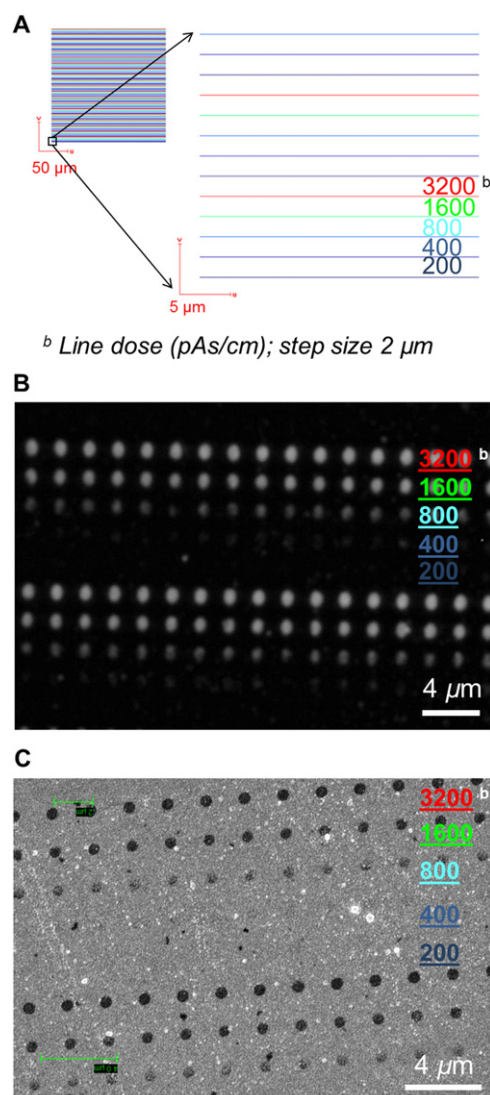
EBL can be performed in area, line and dot exposure modes. The dot exposure mode can be used to fabricate FN nanodots; however, in this mode the exposure times are long since the beam moves to each point exposes and then moves to the next point. To overcome this limitation, line exposure mode was used with step sizes that matched the desired spacings between FN nanodots (figure 3). In this mode, the exposure time was significantly reduced. In addition, FN nanodots with micrometer scale spacings were successfully fabricated on K-casein:ITO-glass. Line exposure was performed at both $30 \, \mu m$ and $7.5 \, \mu m$ apertures (figure 3, online figure S1, available at stacks.iop.org/MRX/1/025402/mmedia). As for area exposure, immunofluorescence signal increased as the electron dose increased. At $30 \, \mu m$ aperture, line doses of 200, 400, 800, 1600 and $3200 \, pAs \, cm^{-1}$ were tested. In this case, while diameters of the resulting FN nanodots were similar (588 ± 6 nm for $3200 \, pAs \, cm^{-1}$; 538 ± 14 nm for 1600

Figure 2. Backfilling with FN is dose dependent. (A) Area pattern drawn in EBL software. (B) Immunofluorescence image of FN squares on K-casein background corresponding to pattern in (A). Sample was stained with FN specific antibodies. (C) Fluorescence intensity and homogeneity of FN immunostaining increased as the applied electron dose increased (n = 4 per dose).

pAs cm^{-1}; 497 ± 18 nm for 800 pAs cm^{-1}) and larger than those at 7.5 μm aperture, the efficiency of backfilling clearly increased as the electron dose increased above 400 pAs cm^{-1} (figure 3). At 7.5 μm aperture, line doses ranging from 2 to 1000 pAs cm^{-1} were tested. Here, FN nanodot diameter significantly increased (from 238 ± 11 nm to 653 ± 18 nm) as the electron dose increased (from 212 pAs cm^{-1} to 1000 pAs cm^{-1}), p < 0.0001 (online figure S1, available at stacks.iop.org/MRX/1/025402/mmedia). The threshold level for initiation of backfilling was determined as 200 pAs cm^{-1} based on intensities of fluorescence images. In addition, area
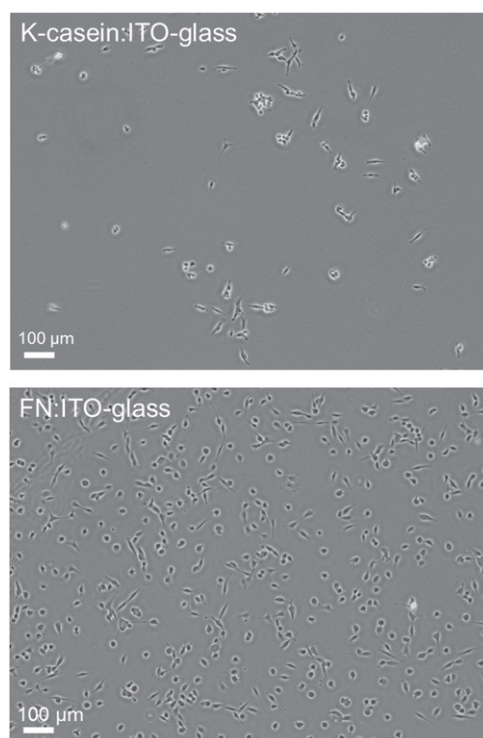
Figure 3. Using a micrometer scale step size in line exposure mode results in nanometer scale FN dots. (A) Line pattern drawn in EBL software. One corner of the pattern is magnified to show individual lines. (B) Immunofluorescence image of FN nanodots on K-casein background corresponding to pattern in (A). Sample was stained with FN specific antibodies. Fluorescence intensity of FN immunostaining increased as the applied dose increased. (C) SEM image of the sample in (B). 30 μm aperture was used for EBL.

exposure mode with micrometer scale step sizes was successfully used to fabricate FN nanodots on K-casein:ITO-glass although the spacings in the x and y directions had to be identical (data not shown).

Previous work has shown that proteins patterned on silicon using this EBL approach are functional at the cellular level as cortical cells, fibroblasts and endothelial cells specifically adhere to FN micro- and nanopatterns. Here, breast cancer cells were cultured on the control and patterned surfaces. Since ITO-glass is transparent, cells on them can easily be visualized using techniques such as phase-contrast microscopy (figure 4). As expected, few cells were

Figure 4. Phase-contrast images of MDA-MB-231 breast cancer cells cultured on transparent ITO-glass surfaces. Top: K-casein:ITO-glass, bottom: FN:ITO-glass.
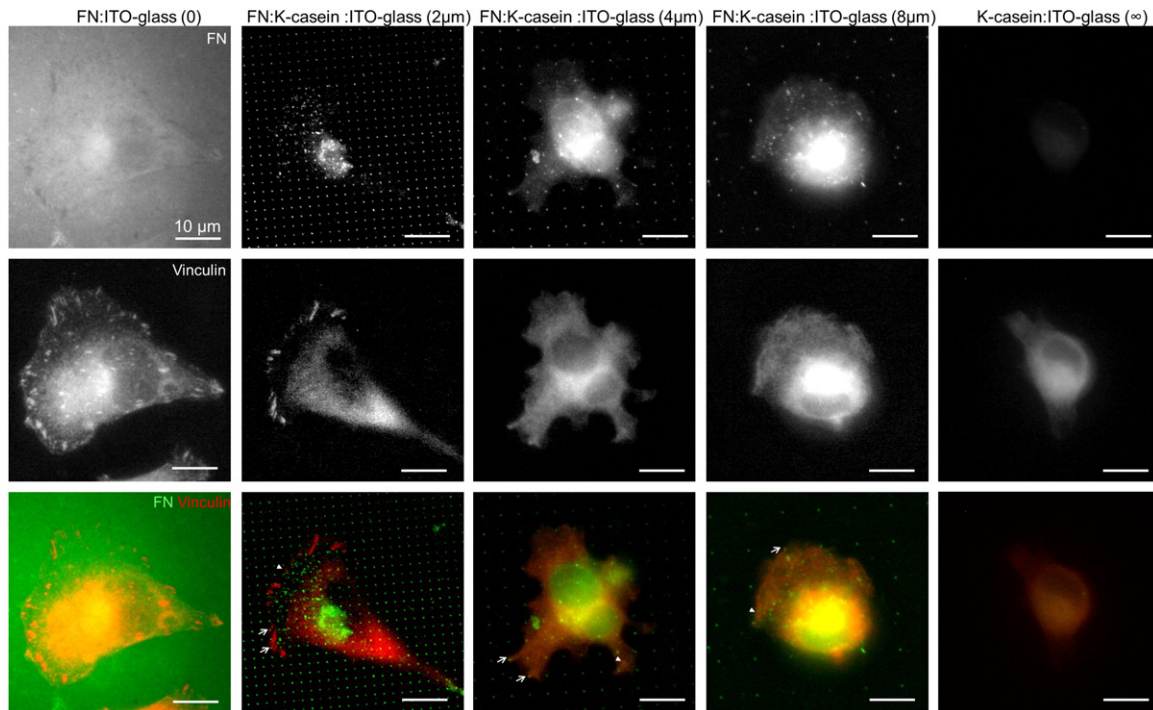
attached and even fewer were spread on K-casein coated ITO-glass while many cells were attached and spread on FN coated ITO-glass.

To evaluate cell adhesion on FN nanodots with micrometer scale spacings, cells were cultured overnight on FN:ITO-glass, K-casein:ITO-glass and FN:K-casein:ITO-glass (i.e. ITO-glass coated with K-casein, exposed to EBL and backfilled with FN), fixed and processed for immunofluorescence. Sample immunofluorescence images are shown in figure 5. Fluorescence signal from the endogenous FN at the perinuclear region is observed in addition to the FN pattern. FAs were detected by immunofluorescence staining of vinculin, which is a well-known marker of FAs. Cells on FN:ITO-glass formed prominent FA while cells on K-casein:ITO-glass did not. Cells on FN:K-casein:ITO-glass also showed FA formation. When the FN nanodots were 200 nm in diameter, cells did not form FAs, consistent with previous results [18]. Cell adhesion was observed on FN nanodots with larger diameters such as 400 or 800 nm. The micrometer scale spacings tested here were up to 8 μm, at which point the cell morphology and FA features were similar to those on K-casein surfaces. Therefore, larger spacings were not tested.
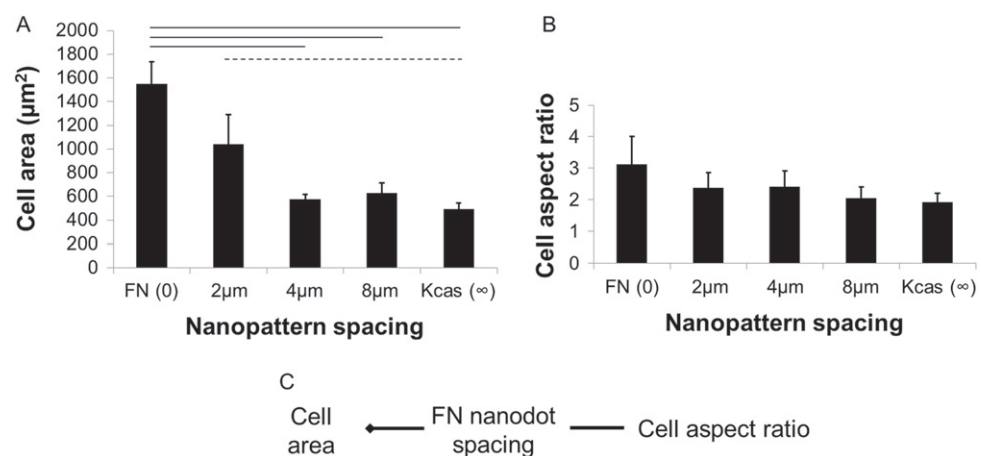
Cell morphology was analyzed as a function of the nanopattern spacing (i.e. the step size in line exposure mode). Cell area correlated negatively with nanopattern spacings: from 1549 $\pm$ 185 μm^2 for FN (0) to 629 $\pm$ 84 μm^2 for 8 μm (R = $-$0.83) to 494 $\pm$ 52 μm^2 for K-casein (∞) (R = $-$0.46) (figure 6(A)). For nanopattern spacings of 4 μm or larger, cell areas did not show any statistically significant further decreases. These data show that nanopattern spacing negatively correlated with cell area and did not change cellular aspect ratio.

Next, FAs were analyzed as a function of the nanopattern spacing. This analysis is outlined with sample images in online figure S2, available at stacks.iop.org/MRX/1/025402/mmedia.
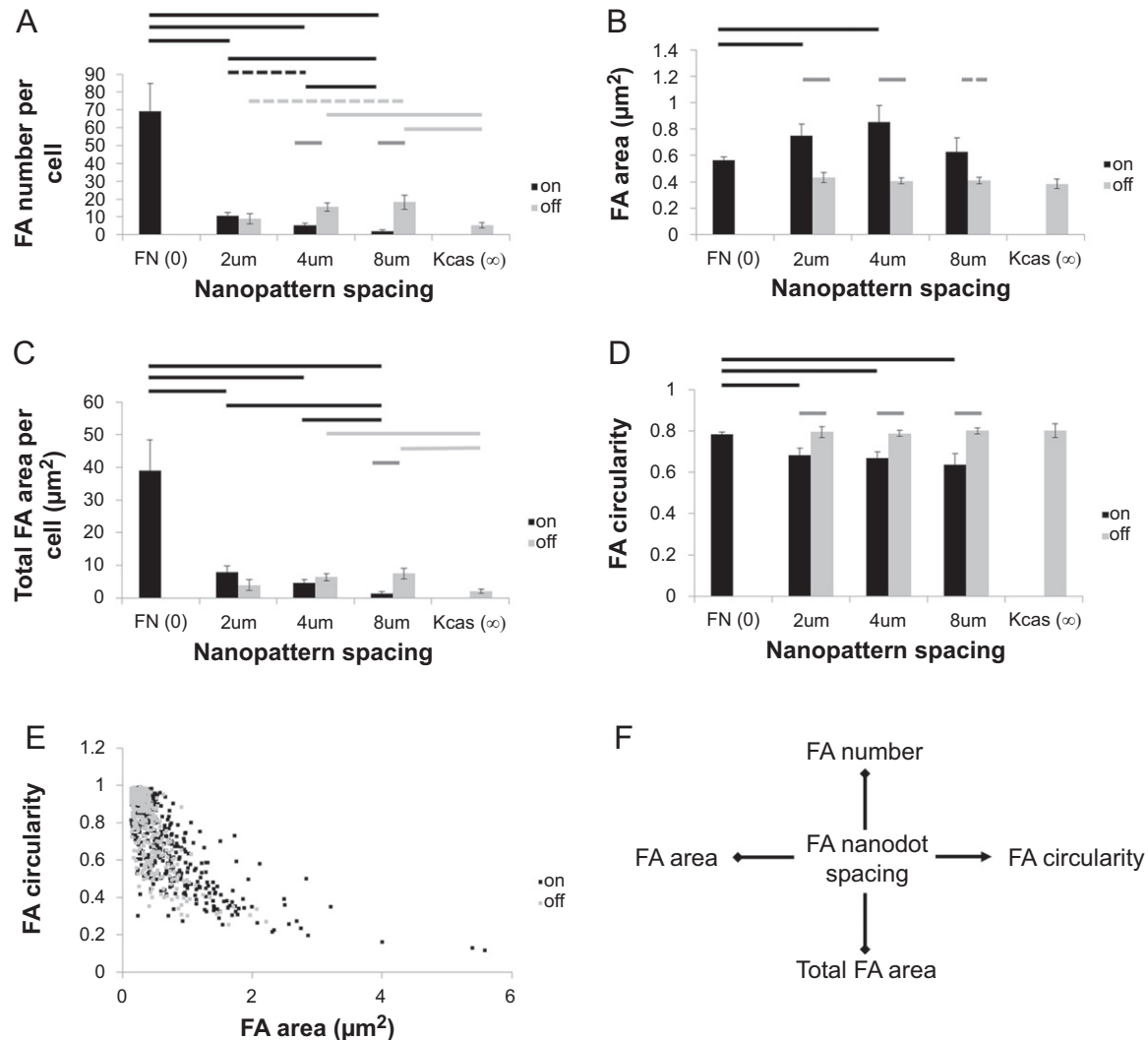
Figure 5. Immunofluorescence images of cells on ITO-glass surfaces. Top, middle and bottom panels show FN, vinculin and merged images, respectively. Prominent FAs are observed in cells cultured on both FN:ITO-glass and FN:K-casein:ITO-glass with 2 μm spacing. FAs are not observed in cells cultured on K-casein:ITO-glass. A few of the FAs on and off FN nanodots are indicated with arrows and arrowheads, respectively.

Figure 6. Nanopattern spacing regulates cell morphology. (A) Cell area decreased as nanopattern spacing increased. (B) Cell aspect ratio did not change significantly with nanopattern spacing. (C) FN nanodot spacing negatively correlated with cell area (━━◆), but did not change cell aspect ratio significantly (▬▬▬). Horizontal solid and dashed lines show data with statistically significant differences with $p < 0.05$ for two-tailed and one-tailed t-tests, respectively.

Figure 7. Nanopattern spacing regulates FAs. (A) Number of FAs on FN per cell decreased as nanopattern spacing increased. Number of FA off FN did not change with nanopattern spacing. (B) Areas of FAs on FN decreased as nanopattern spacing increased from 4 μm to infinity. Areas of FAs off FN were smaller than those on FN. (C) Total FA area on FN per cell decreased as nanopattern spacing increased. Total FA area off FN per cell did not change with nanopattern spacing. (D) FA circularity decreased as nanopattern spacing increased. (E) FA circularity negatively correlated with FA area for all groups. (F) FN nanodot spacing negatively correlated with FA number, FA area, total FA area (——▶), and positively correlated with FA circularity (——▶). Black, dark grey and light grey horizontal lines, show statistically significant differences between FAs with different spacings on FN nanodots, between FAs with different spacings off FN nanodots and between FAs on and off FN nanodots with the same nanopattern spacings, respectively. Horizontal solid and dashed lines show data with statistically significant differences with $p < 0.05$ for two-tailed and one-tailed t-tests, respectively.

Briefly, the vinculin images were processed through a series of steps to remove background and finally thresholded to identify individual FAs. The identified FAs were then mapped on the corresponding FN pattern image to determine FAs on and off FN nanodots. Here 'FA off FN' refers to FA located between FN nanodots rather than on FN nanodots; FAs that form on control FN surfaces are all 'on' FN while those on control K-casein surfaces are all 'off' FN. Different thresholds and background subtraction steps were tested but different paths only negligibly changed the absolute values for the parameters tested and the correlations between parameters were virtually the same (figure 7, online figures S2, S3 and S4, available at stacks. iop.org/MRX/1/025402/mmedia). The number of FAs, the area of FAs, the total area of FAs per cell and the circularity of FA were analyzed (figure 7 and online table S1, available at stacks. iop.org/MRX/1/025402/mmedia). The number of FAs on FN per cell decreased as nanopattern spacing increased (figure 7(A)). Number of FAs off FN did not change with nanopattern spacing. The numbers of FAs off FN were higher than those on FN when the nanopattern spacing was $4\,\mu$m and $8\,\mu$m. On the other hand, areas of individual FAs on FN decreased as nanopattern spacing increased from $2\,\mu$m to infinity (K-casein) (figure 7(B)). Areas of FA on FN:ITO-glass ($0.56 \pm 0.03\,\mu$m^2) for the breast cancer cell line used in this study were consistent with previously reported values on uniform surfaces [39]. Areas of FA on FN:ITO-glass were smaller than those on FN:K-casein:ITO-glass with nanopattern spacings of $2\,\mu$m and $4\,\mu$m. Areas of FAs off FN were smaller than those on FN for all nanopattern spacings, namely, 2, 4 and $8\,\mu$m. Areas of FAs off FN did not change with nanopattern spacing. What is more, total FA area on FN per cell decreased as nanopattern spacing increased (figure 7(C)). Total FA area off FN per cell did not change with nanopattern spacing. Furthermore, FAs are known to gain an elongated shape as they increase in size and mature [2, 4]. FA circularity on FN had an inverse correlation with micrometer scale spacing ($R = -0.88$) (figure 7(D)). FA circularity off FN nanodots was higher than that on FN nanodots. FA circularity negatively correlated with FA area for all groups, as expected ($R = -0.73$) (figure 7(E)). These data show that nanopattern spacing negatively correlated with FA number, FA area and total FA area per cell while it positively correlated with FA circularity. Interestingly, when the total area for all FAs was expressed as a percentage of cell area, MDA-MB-231 cells on FN:ITO-glass surfaces employed only $2.5 \pm 0.5\%$ of their total area to form FAs. For nanopatterned surfaces, this value dropped down to $\sim1.7 \pm 0.2\%$. These results show that, first, the cells can form FAs, though fewer and smaller, off FN nanodots. This observation is expected considering that cells can secrete their own FN during an overnight culture and that serum present in the culture medium contains FN. Second, when FN is uniformly available on the surface, cells form many and small Fas, whereas cells focus on the available FN areas and form fewer and larger FAs on nanopatterned surfaces as long as the nanopattern spacing is equal to or smaller than $4\,\mu$m. Third, the major features examined in this work appear to significantly change when the nanopattern spacing goes higher than $4\,\mu$m, suggesting this value as a threshold for spacings of adhesive nanopatterns. Fourth, cells on 2D surfaces use only 1.5–3% of their projected area for forming adhesions.

Conclusions

This study shows that patterns of proteins that mimic the *in vivo* ECM organization can be directly fabricated on transparent ITO-glass using EBL. In addition, micrometer scale spacings of 2, 4 and $8\,\mu$m between fibronectin nanodots are shown to regulate cell adhesion through

modification of cell area, FA number, size and circularity. Overall, cell behavior shifts at the apparent threshold of 4 *μ*m spacing. These results will assist in the design and fabrication of surfaces mimicking the *in vivo* organization of ECM and will promote further studies on cell adhesion, migration and ECM modification, comparing health and disease states.

Acknowledgements

References

[1] Berrier A L and Yamada K M 2007 Cell-matrix adhesion *J. Cell Physiol.* **213** 565–73

[2] Zaidel-Bar R, Cohen M, Addadi L and Geiger B 2004 Hierarchical assembly of cell-matrix adhesion complexes *Biochem. Soc. Trans.* **32** 416–20

[3] Zaidel-Bar R, Itzkovitz S, Ma'ayan A, Iyengar R and Geiger B 2007 Functional atlas of the integrin adhesome *Nat. Cell Biol.* **9** 858–68

[4] Zamir E and Geiger B 2001 Molecular complexity and dynamics of cell-matrix adhesions *J. Cell Sci.* **114** 3583–90

[5] Kim D H, Provenzano P P, Smith C L and Levchenko A 2012 Matrix nanotopography as a regulator of cell function *J. Cell Biol.* **197** 351–60

[6] Provenzano P P, Eliceiri K W and Keely P J 2009 Multiphoton microscopy and fluorescence lifetime imaging microscopy (FLIM) to monitor metastasis and the tumor microenvironment *Clin. Exp. Metastasis* **26** 357–70

[7] Soucy P A and Romer L H 2009 Endothelial cell adhesion, signaling, and morphogenesis in fibroblast-derived matrix *Matrix Biol.* **28** 273–83

[8] Wolf K, Alexander S, Schacht V, Coussens L M, von Andrian U H, van Rheenen J *et al* 2009 Collagen-based cell migration models *in vitro* and *in vivo Semin. Cell Dev. Biol.* **20** 931–41

[9] Zoumi A, Yeh A and Tromberg B J 2002 Imaging cells and extracellular matrix *in vivo* by using second-harmonic generation and two-photon excited fluorescence *Proc. Nat. Acad. Sci. USA* **99** 11014-9

[10] Alsberg E, Feinstein E, Joy M P, Prentiss M and Ingber D E 2006 Magnetically-guided self-assembly of fibrin matrices with ordered nano-scale structure for tissue engineering *Tissue Eng.* **12** 3247–56

[11] Cavalcanti-Adam E A, Volberg T, Micoulet A, Kessler H, Geiger B and Spatz J P 2007 Cell spreading and focal adhesion dynamics are regulated by spacing of integrin ligands *Biophys. J.* **92** 2964–74

[12] Chen C S, Mrksich M, Huang S, Whitesides G M and Ingber D E 1997 Geometric control of cell life and death *Science* **276** 1425–8

[13] Deeg J A, Louban I, Aydin D, Selhuber-Unkel C, Kessler H and Spatz J P 2011 Impact of local versus global ligand density on cellular adhesion *Nano Lett.* **11** 1469–76

[14] Gingras J, Rioux R M, Cuvelier D, Geisse N A, Lichtman J W, Whitesides G M *et al* 2009 Controlling the orientation and synaptic differentiation of myotubes with micropatterned substrates *Biophys. J.* **97** 2771–9

[15] Lutz R, Pataky K, Gadhari N, Marelli M, Brugger J and Chiquet M 2011 Nano-stenciled RGD-gold patterns that inhibit focal contact maturation induce lamellipodia formation in fibroblasts *Plos One* **6**

[16] Oliva A A, James C D, Kingman C E, Craighead H G and Banker G A 2003 Patterning axonal guidance molecules using a novel strategy for microcontact printing *Neurochem. Res.* **28** 1639–48

[17] Park J, Kim H N, Kim D H, Levchenko A and Suh K Y 2012 Quantitative analysis of the combined effect of substrate rigidity and topographic guidance on cell morphology *IEEE Trans. NanoBiosci.* **11** 28–36

[18] Pesen D and Haviland D B 2009 Modulation of cell adhesion complexes by surface protein patterns *ACS Appl. Mater. Interfaces* **1** 543–8

[19] Tat J R, Shi L F, Deng Z, Lo S H and Liu G Y 2012 Nanostructures of designed geometry and functionality enable regulation of cellular signaling processes *Biochemistry* **51** 5876–93

[20] Agheli H, Malmstrom J, Larsson E M, Textor M and Sutherland D S 2006 Large area protein nanopatterning for biological applications *Nano Lett.* **6** 1165–71

[21] Biggs M J P, Richards R G and Dalby M J 2010 Nanotopographical modification: a regulator of cellular function through focal adhesions *Nanomed.-Nanotechnol. Biol. Med.* **6** 619–33

[22] Elineni K K and Gallant N D 2011 Regulation of cell adhesion strength by peripheral focal adhesion distribution *Biophys. J.* **101** 2903–11

[23] Malmstrom J, Lovmand J, Kristensen S, Sundh M, Duch M and Sutherland D S 2011 Focal complex maturation and bridging on 200 nm vitronectin but not fibronectin patches reveal different mechanisms of focal adhesion formation *Nano Lett.* **11** 2264–71

[24] Geiger B, Spatz J P and Bershadsky A D 2009 Environmental sensing through focal adhesions *Nat. Rev. Mol. Cell Biol.* **10** 21–33

[25] Piner R D, Zhu J, Xu F, Hong S H and Mirkin C A 1999 Dip-pen nanolithography *Science* **283** 661–3

[26] Lussi J W, Tang C, Kuenzi P A, Staufer U, Csucs G, Voros J *et al* 2005 Selective molecular assembly patterning at the nanoscale: a novel platform for producing protein patterns by electron-beam lithography on SiO$_2$/indium tin oxide-coated glass substrates *Nanotechnology* **16** 1781–6

[27] Lussi J W, Michel R, Reviakine I, Falconnet D, Goessl A, Csucs G *et al* 2004 A novel generic platform for chemical patterning of surfaces *Prog. Surf. Sci.* **76** 55–69

[28] Harnett C K, Satyalakshmi K M and Craighead H G 2001 Bioactive templates fabricated by low-energy electron beam lithography of self-assembled monolayers *Langmuir* **17** 178–82

[29] Hoa X D, Martin M, Jimenez A, Beauvais J, Charette P, Kirk A *et al* 2008 Fabrication and characterization of patterned immobilization of quantum dots on metallic nano-gratings *Biosens. Bioelectron.* **24** 970–5

[30] Palankar R, Medvedev N, Rong A and Delcea M 2013 Fabrication of quantum dot microarrays using electron beam lithography for applications in analyte sensing and cellular dynamics *ACS Nano* **7** 4617–28

[31] Pesen D, Erlandsson A, Ulfendahl M and Haviland D B 2007 Image reversal for direct electron beam patterning of protein coated surfaces *Lab on a Chip.* **7** 1603–6

[32] Pesen D, Heinz W F, Werbin J L, Hoh J H and Haviland D B 2007 Electron beam patterning of fibronectin nanodots that support focal adhesion formation *Soft Matter.* **3** 1280–4

[33] Ron A, Lee G H, Amar L, Ghassemi S and Hone J 2011 Adjacent assembly of self-assembled monolayers for the construction of selective bio-platforms *Sensors Actuators* **159** 75–81

[34] Rundqvist J, Mendoza B, Werbin J L, Heinz W F, Lemmon C, Romer L H *et al* 2007 High fidelity functional patterns of an extracellular matrix protein by electron beam-based inactivation *J. Am Chem. Soc.* **129** 59–67

[35] Alonso J M, Ondarcuhu T and Bittner A M 2013 Integration of plant viruses in electron beam lithography nanostructures *Nanotechnology* **24** 105305

[36] Pesen D, Erlandsson A, Ulfendahl M and Haviland D B 2007 Image reversal for direct electron beam patterning of protein coated surfaces *Lab on a Chip.* **7** 1603–6

[37] Pesen D, Heinz W F, Werbin J L, Hoh J H and Haviland D B 2007 Electron beam patterning of fibronectin nanodots that support focal adhesion formation *Soft Matter.* **3** 1280–4

[38] Seshadri K, Froyd K, Parikh A N, Allara D L, Lercel M J and Craighead H G 1996 Electron-beam-induced damage in self-assembled monolayers *J. Phys. Chem.* **100** 15900–9

[39] Gu W, Katz Z, Wu B, Park H Y, Li D L, Lin S *et al* 2012 Regulation of local expression of cell adhesion and motility-related mRNAs in breast cancer cells by IMP1/ZBP1 *J. Cell Sci.* **125** 81–91